3D subsurface modeling at Limburg using multimodal surface waves

S. Koley, X. Campman, M. Fays, M. Hadrien, S. Kadmiel, M. Kiehn, F. Nguyen, S. Peters, W. Walk

Motivation

- Why do we need a 3D subsurface model?
  - Understanding distribution of elastic properties of the subsurface
    - Help with excavation, tunneling, etc.
    - Decide on the location of the vertices – Hard rock very close to the surface is not suitable for attenuation of noise generated on the surface
    - Suitability of rocks for hosting caverns
  - 3D elastic wave equation simulation
    - Subsurface model for P, S-wave and density is necessary
    - First stage for Newtonian noise simulation
- Are boreholes not important?
  - Mapping between surface wave velocities and underground S-wave model is non-unique
    - P and S-wave velocities from borehole logging are used to constrain the parameter space
    - Understanding lithology and stratigraphy to constrain depth-space

Sensor network – An array of 183 vertical component 5 Hz geophones were deployed between November 13 and December 03, 2020

- Out of the 183 geophone, 169 used in the analysis
  - Some geophones stopped working shortly after deployment
  - Low-frequency distortion – software bug
- Array aperture $\approx 6 \times 7$ sq. km
- Recording specification: 500 sps, 24 dB gain

Fig1:Wireless Innoseis sensors equipped with 5 Hz geophones and a self-noise of $1\ \mathrm{ng}/\sqrt{\mathrm{Hz}}$ at 1 Hz [1]

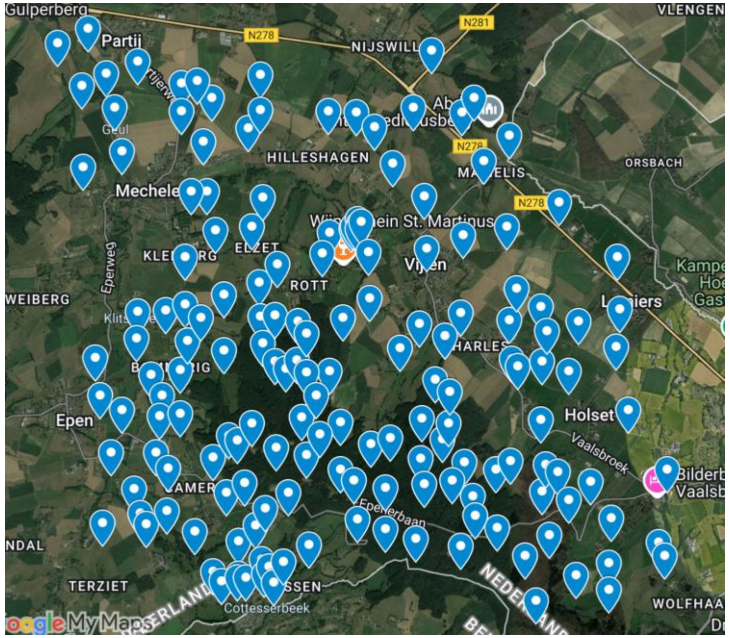

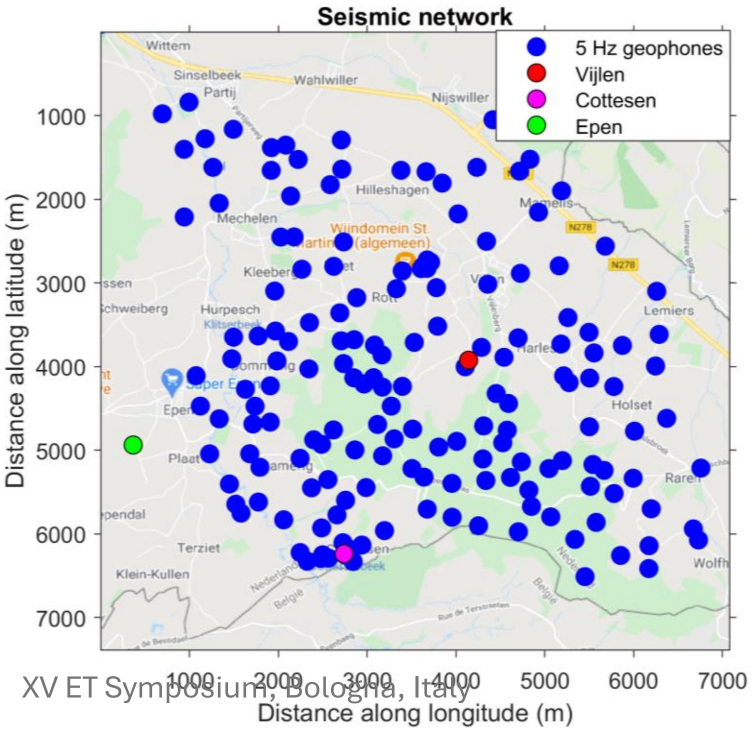

Fig2: (left) Location of the 169 geophones shown on a map of the region. (right) Location of the geophones shown in cartesian coordinates overlayed on a map of the region. The red, magenta, and the green solid circles show the location of the boreholes in the region of study

Geological context – The geology at Terziet is characterized by a transition from soft-soil to hard rock between depths of 40-60 meters

- Lithology
  - < 20 m - soft sand clay
  - < 60 m – Upper cretaceous – soft limestones
  - < 300 m – Namurian formation – Mudstones and sandstones
  - > 300 m - Fammenian formation – Hard micaceous sandstones

- Sonic log interpretation
  - Logging possible depths greater than 50 m
  - Cottesen log – very noisy; transition to velocities between 2 – 2.5 km/s at shallow depths between 50-60 m
  - Epen and Vijlen – transition to S-wave velocities between 2 and 2.5 km/s a greater depths of about 100 m
  - P-wave velocities between 4-5 km/s at depths below 100 m

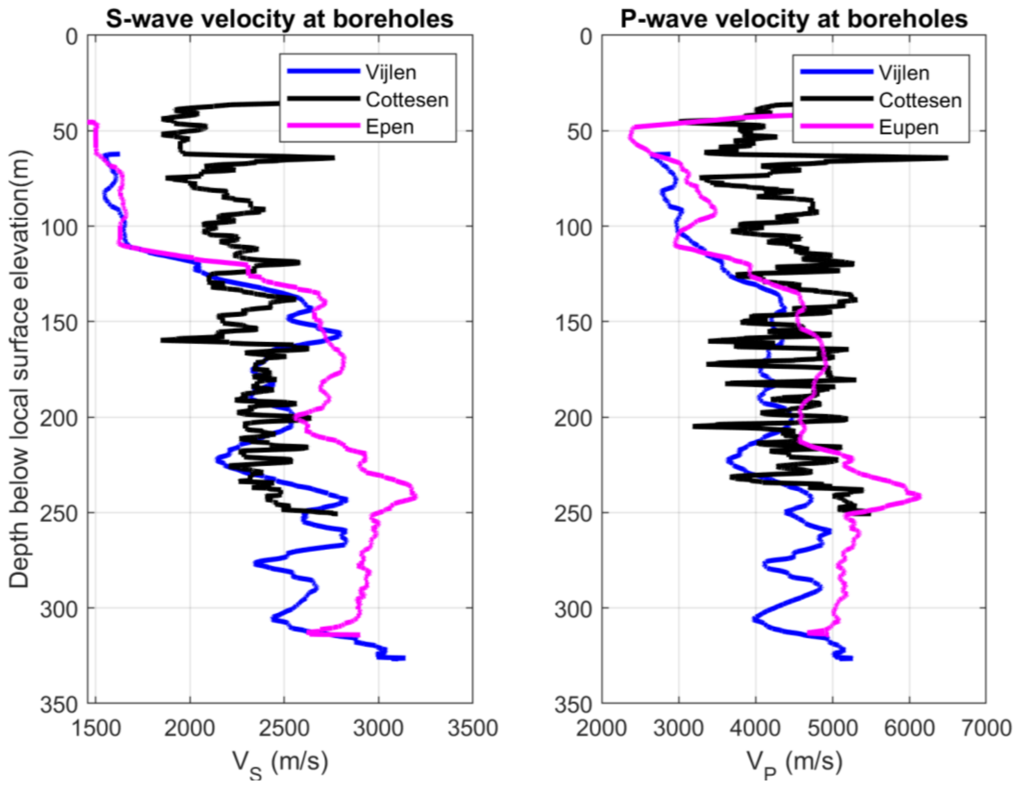

Fig3: (left) The blue, magenta and the black solid curves represent the S-wave velocity logs derived from the boreholes at Vijlen, Cottesen, and Epen. (right) Same as left, but corresponds to P-wave velocities. The Y-axes corresponds to depth below the local surface elevation

LIÈGE université

Noise power characteristics – Stations located near local roads/houses exhibit a typical day/night variation of about 40 dB in power for frequencies above 10 Hz

- PSD parameters
  - Data downsampled to 50 Hz
  - Window length – 600 s, window type – Hann
  - Window overlap length – 300 s

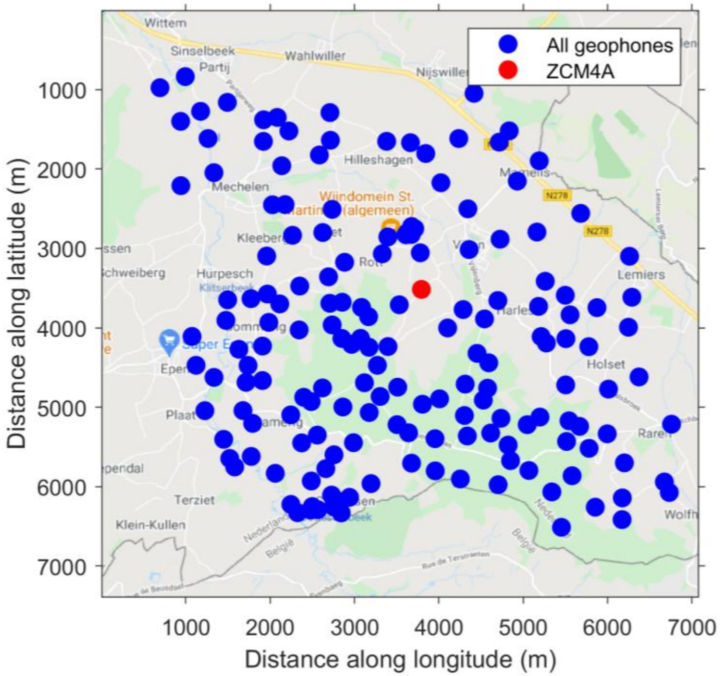

Fig4: The solid red dot shows the location of station ZCM4A in the array

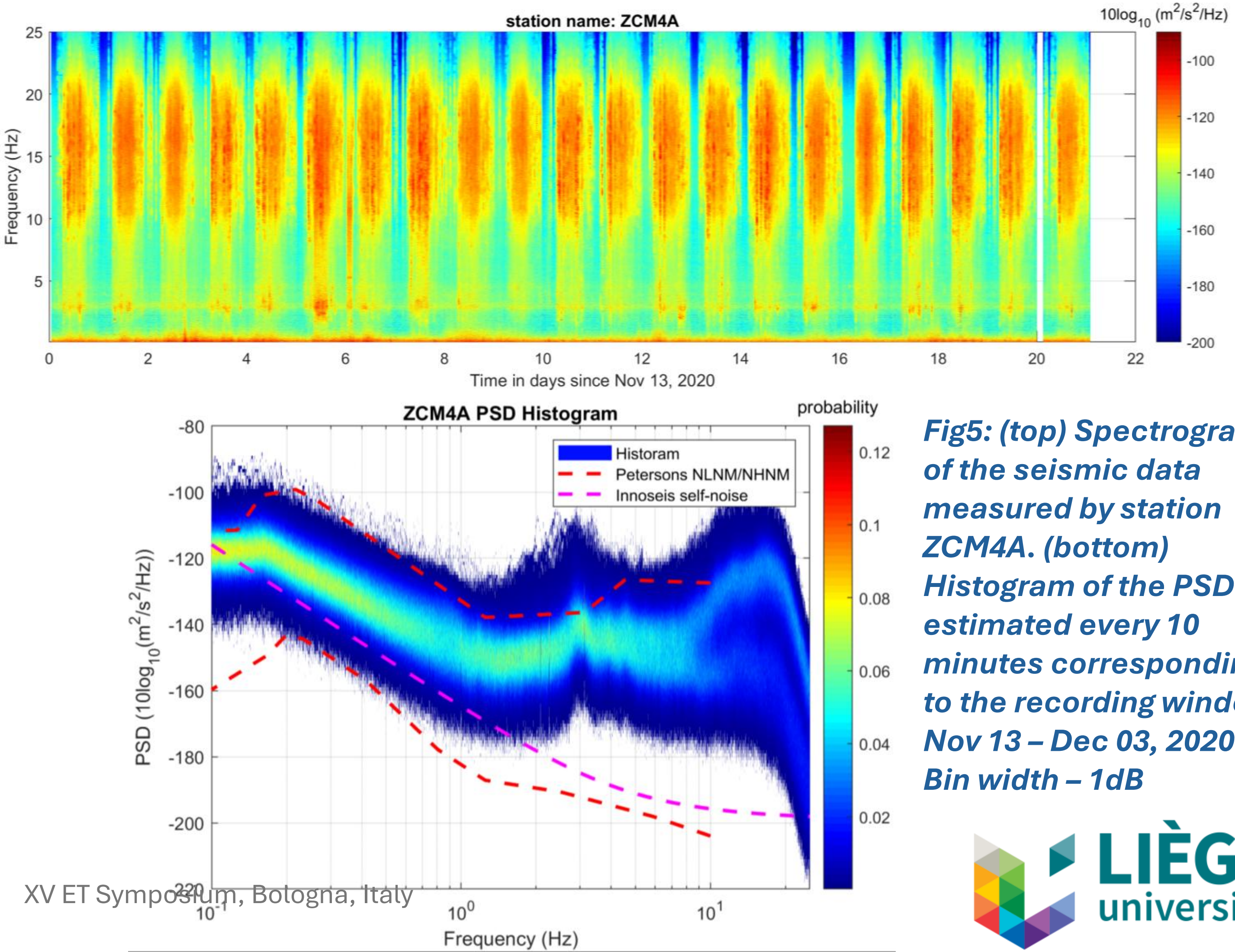

Fig5: (top) Spectrogram of the seismic data measured by station ZCM4A. (bottom) Histogram of the PSD estimated every 10 minutes corresponding to the recording window Nov 13 – Dec 03, 2020. Bin width – 1dB

Average PSD characteristics– Spatial distribution of the PSD for low frequencies shows a correlation with the topography of the region

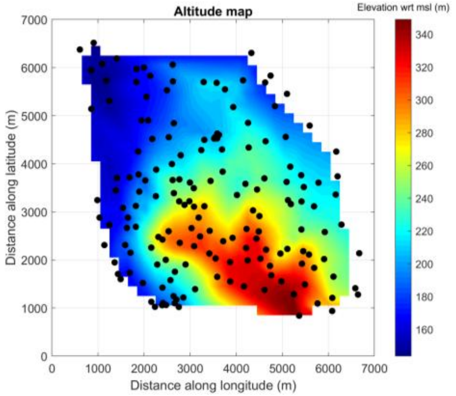

- A lower PSD is observed in the valleys (Panzerra, 2011)
  - Hard rock close to surface reduces reverberation of seismic noise which is typically observed in sedimentary basins

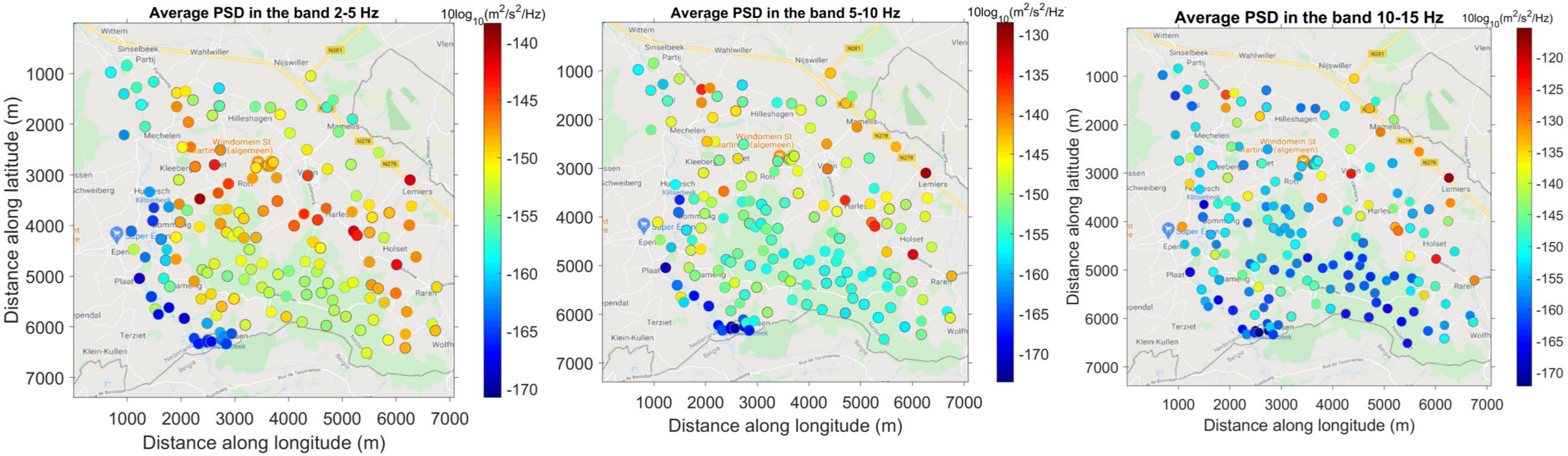

Fig6: (left) Average PSD estimated in the frequency band 2 – 5 Hz shown at the station locations with the colorbar representing the average PSDs. (middle) same as (left), but corresponds to the 5-10 Hz band. (right) same as (left) but corresponds to 10–15 Hz band

Beamforming – Beampowers are estimated in 0.1 Hz wide frequency bands over the interval 1.4 – 2.5 Hz

- Two propagation modes identified
- Slower mode has a almost isotropic direction of propagation – ideal for interferometry
- Higher mode visible for frequencies below 1.5 Hz
- Fundamental or the slowly propagating mode visible for frequencies greater than 1.5 Hz
- Higher mode has strong directional bias – originating North -East

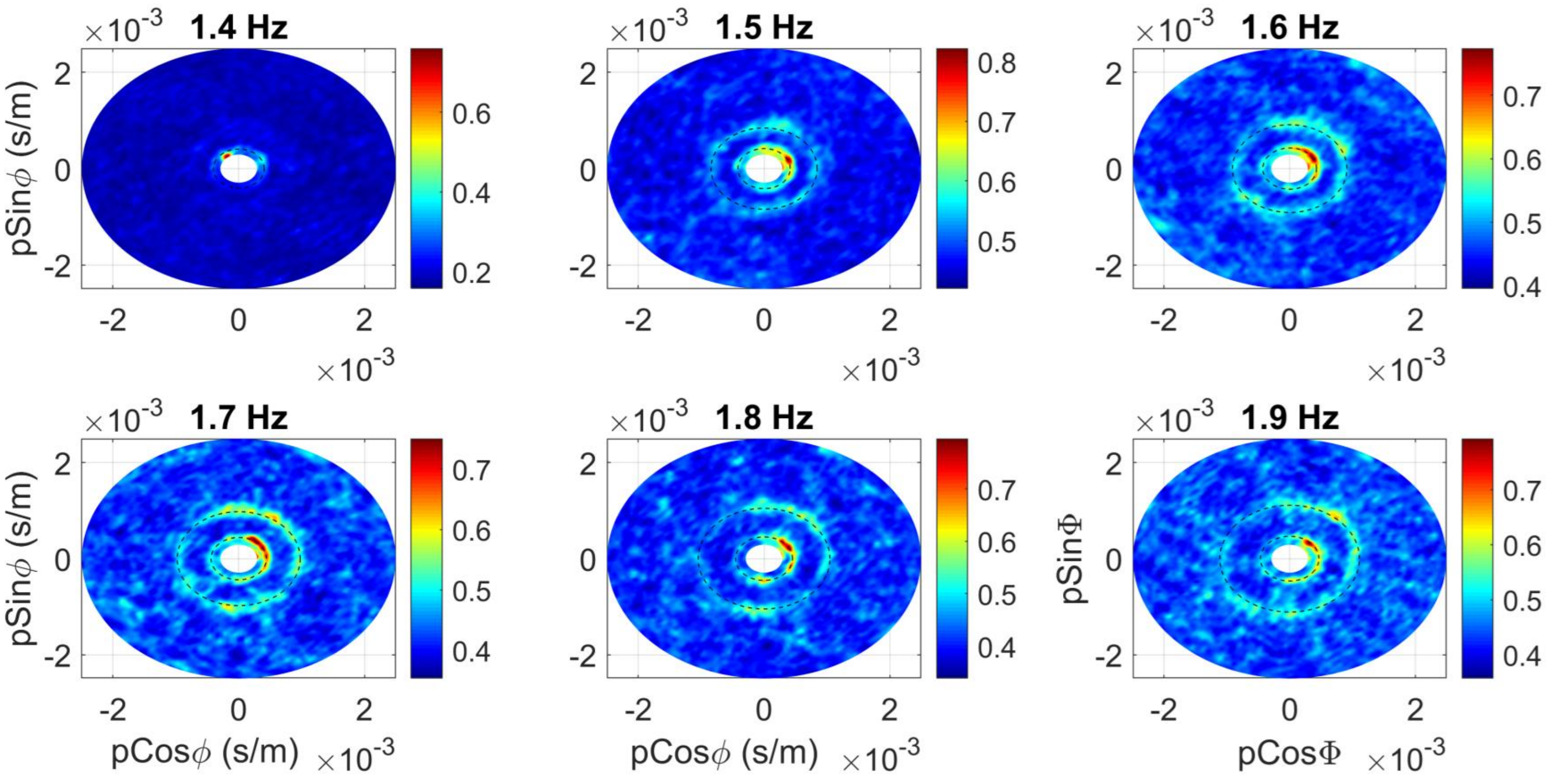

Fig7: Beampower distribution shown in the frequency bands 1.4 – 1.9 Hz. A fast propagating mode with strong directional bias is observed. The slower mode has almost isotropic illumination

Beamforming – Beampowers are estimated in 0.1 Hz wide frequency bands in the range 1.4 – 2.5 Hz

- Faster mode not visible for frequencies above 2 Hz
- Drastic loss of coherence for frequencies > 2.4 Hz

Some pertinent issues

- Fugro treated the slower mode as the fundamental and assumed it to be true for the entire array – Is that the correct way?
- Sisprobe treated the faster mode as the fundamental and the slower mode as an anomaly in the region
- Let's try to figure out what is actually happening ☺

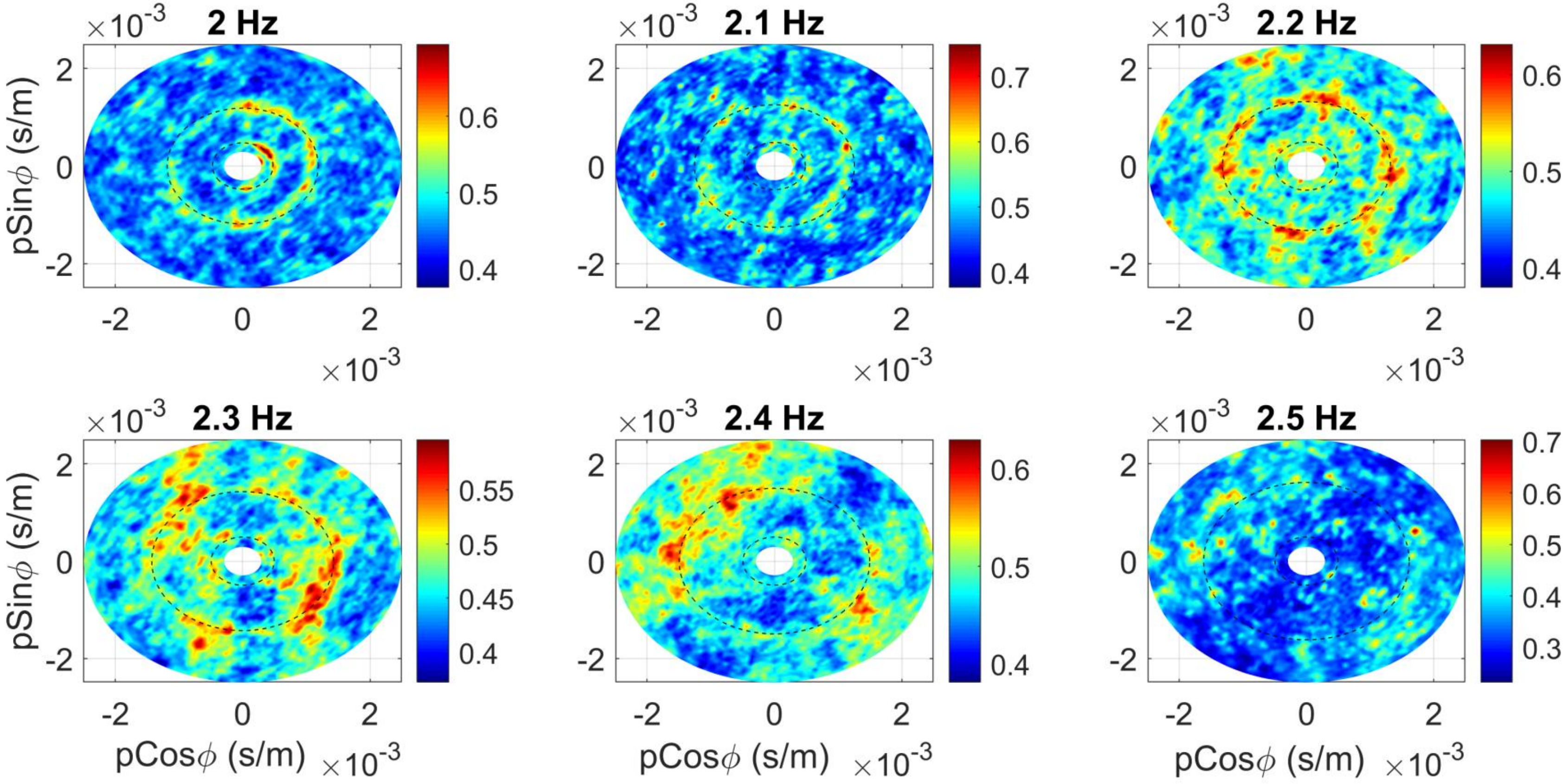

Fig8: Beampower distribution shown in the frequency bands 1.4 – 1.9 Hz. A fast propagating mode with strong directional bias is observed. The slower mode has almost isotropic illumination

Beamforming – Azimuthal summation of the beampower is used to estimate the apparent velocity of propagation

- Faster mode is weakly dispersive between 2 – 2.5 km/s
    - High chances of it being a higher order Rayleigh wave mode or heterogeneity
    - Possibility of mixing between body waves and higher Rayleigh wave modes
- Slower mode shows strong dispersion in the frequency band 1.5 – 2.4 Hz
- Apparent velocities vary between 1.2 – 0.6 km/s

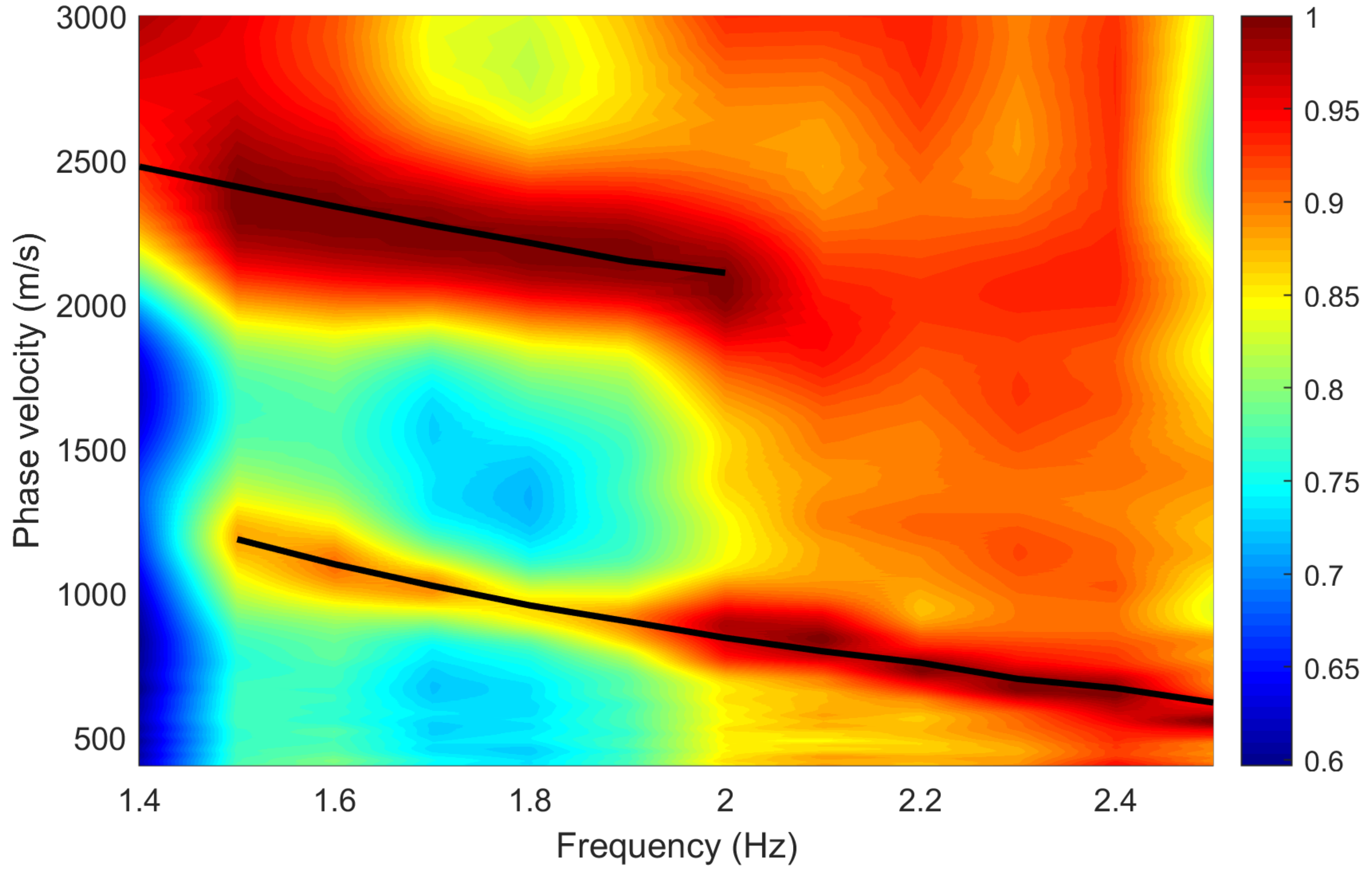

Fig9: Azimuthally averaged beampower expressed as a function of velocity in the frequency band 1.4 – 2.5 Hz. Two propagation modes are identified

Virtual noise gather – correlations for all station pairs are sorted in 25 m distance bins and averaged

- Averaging correlations in distance bins increases the symmetricity of the correlations

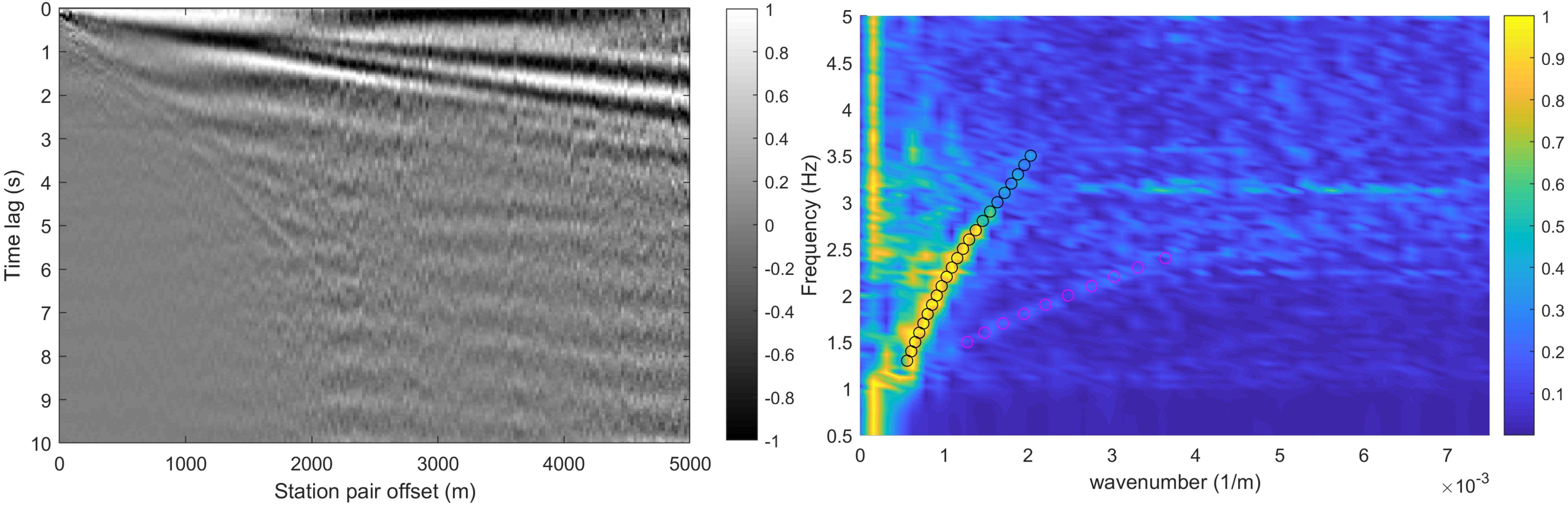

Fig10: (left) Virtual noise gather obtained by stacking cross-correlations in 25 m distance bins. A strong higher mode propagating with group velocities between 1- 2.5 km/s, and a weak fundamental mode propagating between velocities of 0.2 – 0.5 km/s. (right) FK transform of the noise gather with the black and the magenta circles representing the dispersive nature of the fast and slow propagation modes, respectively

Comparison between velocities derived from beamforming and that from the FK analysis of the cross-correlation gather

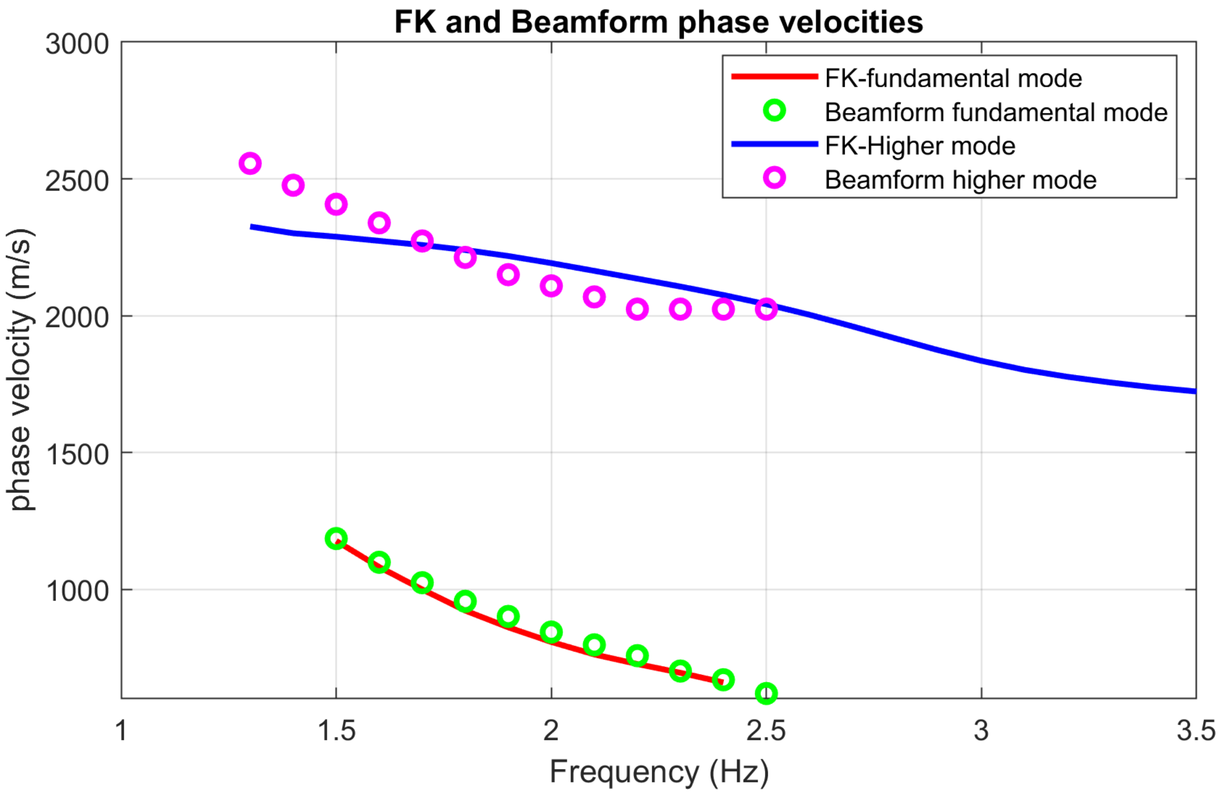

Fig11: Comparison of the apparent velocity of propagation derived from beamforming and FK-analysis

- Velocities derived from beamforming are in reasonable agreement with that derived from the FK analysis of the cross-correlation
    - Small differences arise due to difference in the pre-processing of the ambient noise data
- The phase velocities derived for each of the modes serve as the backbone for the tomography and the inversion that follows
- Important to investigate if these values hold true for the entire array

FK analysis of cross-correlations derived from subarrays – subarray in the North-West reveal strong differences in phase velocities

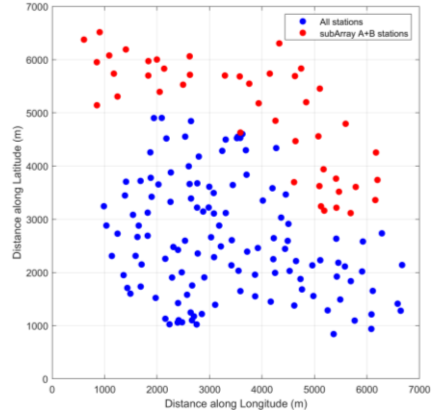

- Phase velocities are much higher compared to phase velocities obtained over the entire array

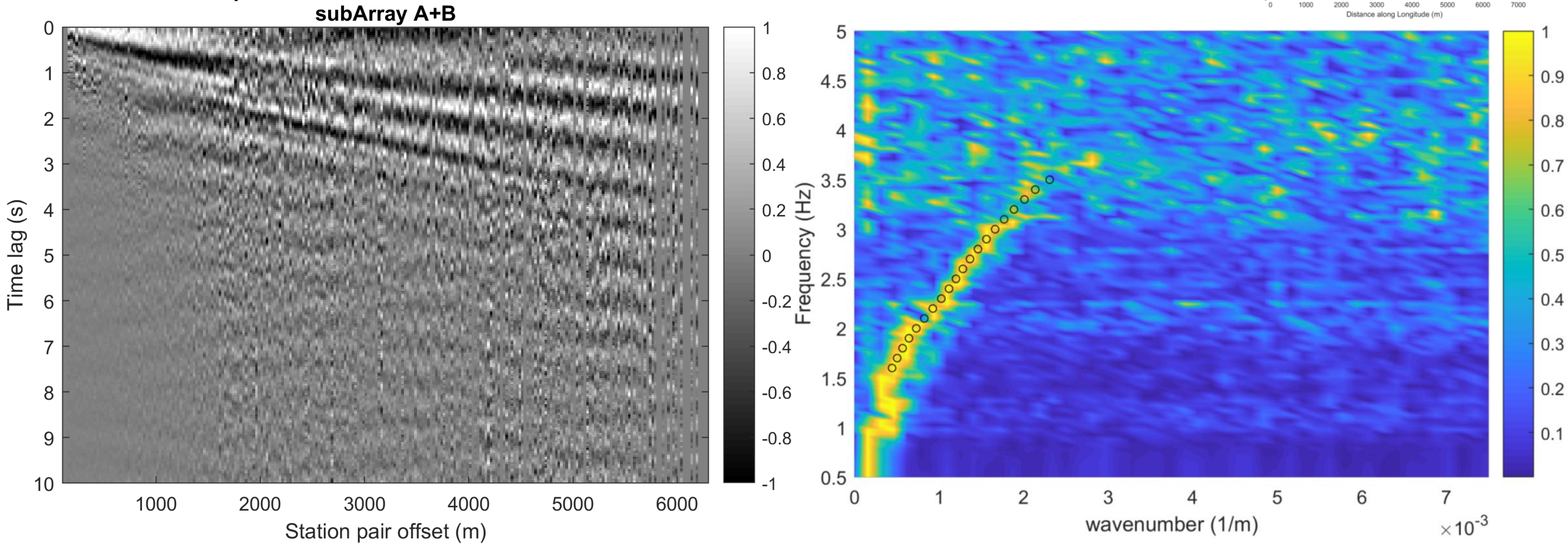

Fig12: (left) Virtual noise gather obtained by stacking cross-correlations in 25 m distance bins. A strong higher mode propagating with group velocities between 1- 2.5 km/s,. (right) FK transform of the noise gather with the black circles representing the dispersive nature of the fast mode

A subarray in the center shows a much slower fundamental mode

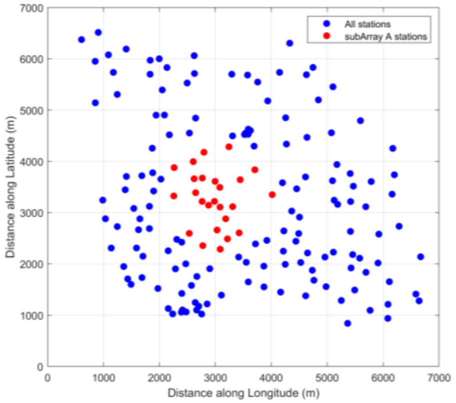

- subArray D, shows a strong fundamental mode

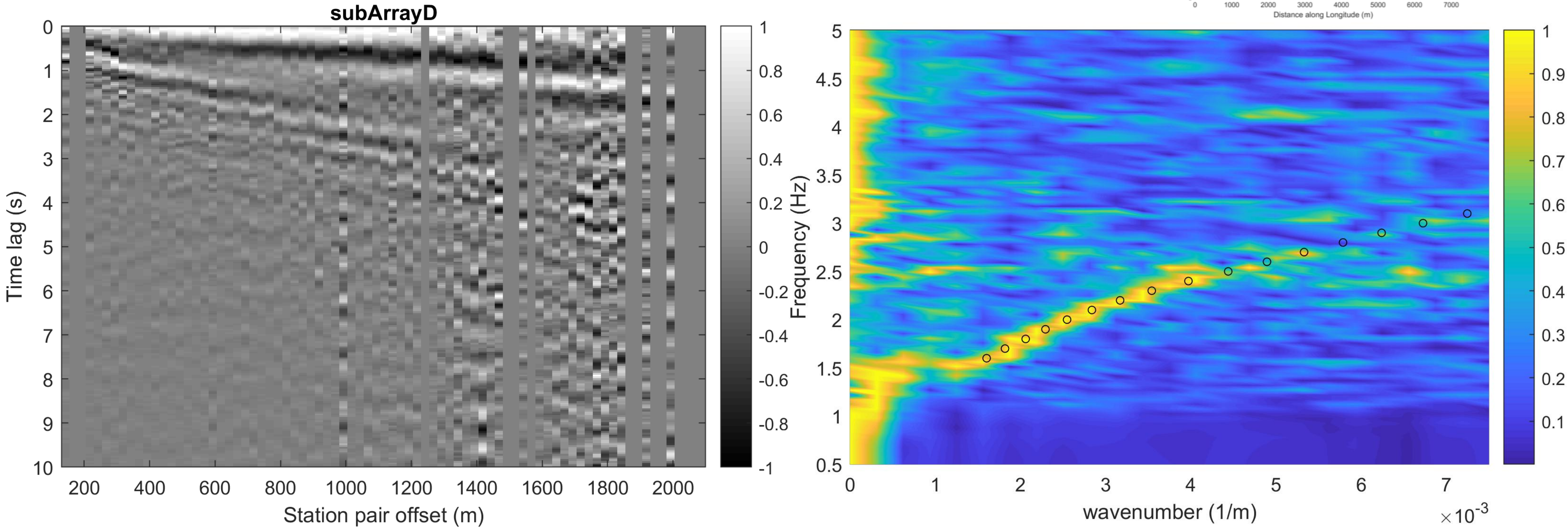

Fig13: (left) Virtual noise gather obtained by stacking cross-correlations in 25 m distance bins. A strong higher mode propagating with group velocities between 0.2- 1 km/s,. (right) FK transform of the noise gather with the black circles representing the dispersive nature of the slower fundamental mode

It was possible to obtain a larger cluster of stations by combining smaller arrays to the south and center of the array that show similar dispersive properties

- subarray of all stations that show a fundamental mode and higher mode

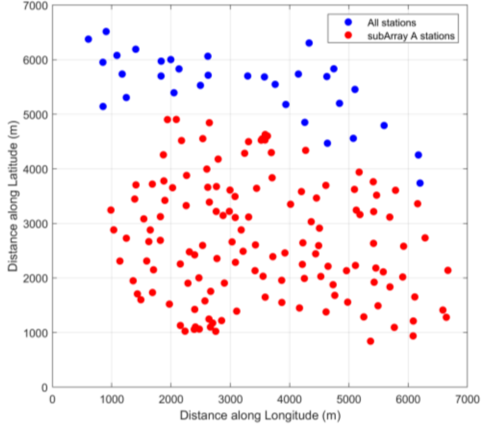

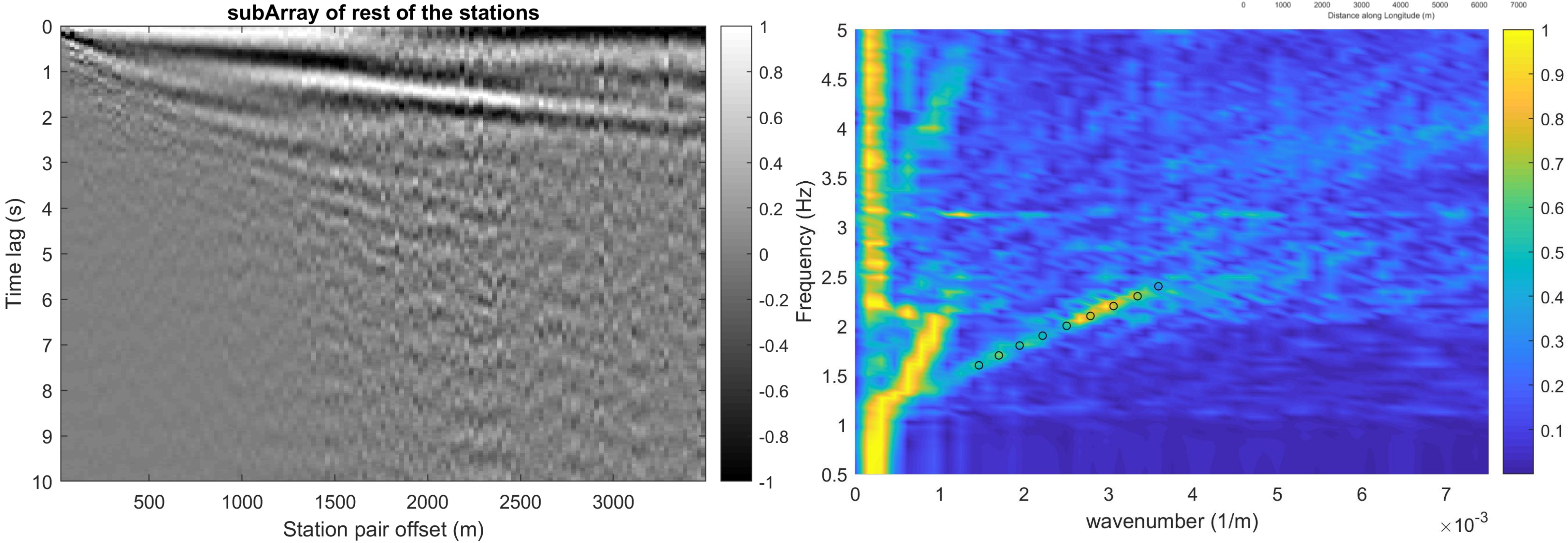

Fig14: (left) Virtual noise gather obtained by stacking cross-correlations in 25 m distance bins. A strong higher mode propagating with group velocities between 0.2- 1 km/s,. (right) FK transform of the noise gather with the black circles representing the dispersive nature of the slower fundamental mode

It was possible to extract a coherent fundamental and a higher mode throughout the southern part of the array

- The weak fundamental mode that was visible in the analysis of the full array is a reasonable representation of the southern parts of the array
- The higher mode with much smaller velocities of 2.5 – 1.5 km/s compared to the northern array is the first overtone observed in the southern array

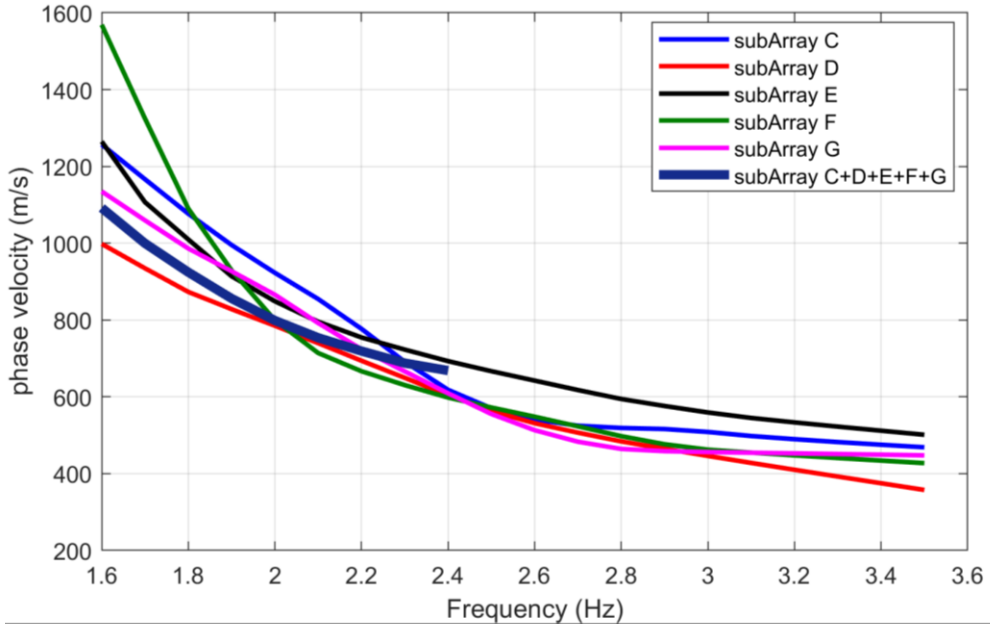

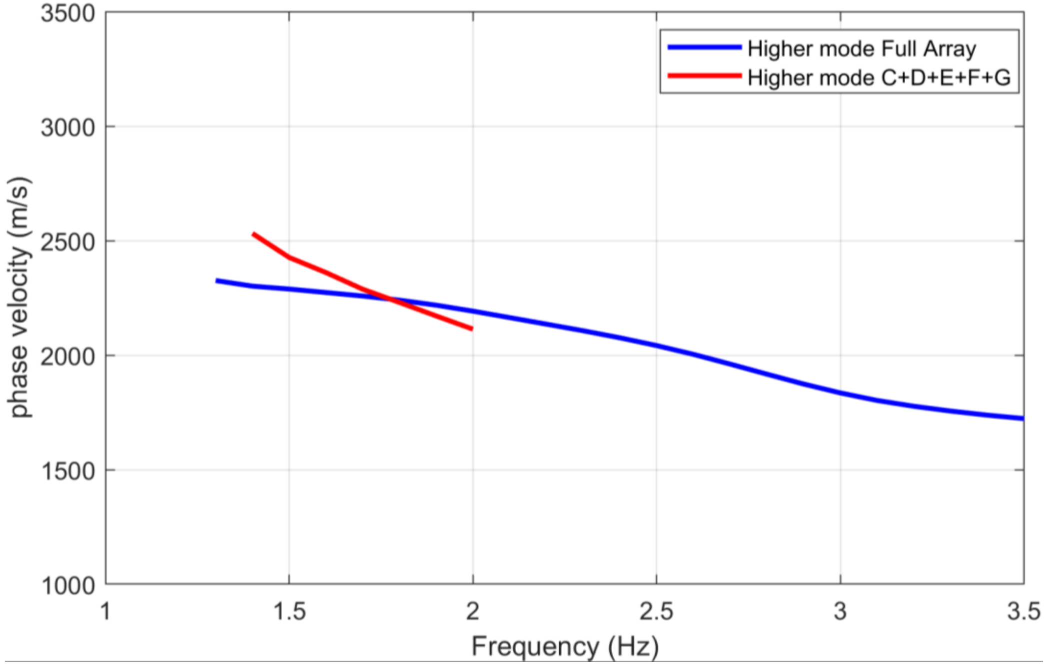

Fig15: (left) Comparison of the fundamental mode phase velocities derived from the subarrays separately and that from the entire southern array. (right) Comparison of the higher mode phase velocities derived from the entire array (blue), and the southern array

Given that we have arrived at a cluster of stations with consistent fundamental and higher mode dispersion we move to group velocity picking

- Frequency-Time analysis performed to estimate group velocity per station pair
- Three checks are made to remove bad group velocity checks
  - Spectral SNR >= 5
  - Station-pair separation >= 600 m
  - Group dispersion curves with at least 50 % valid dispersion points are used

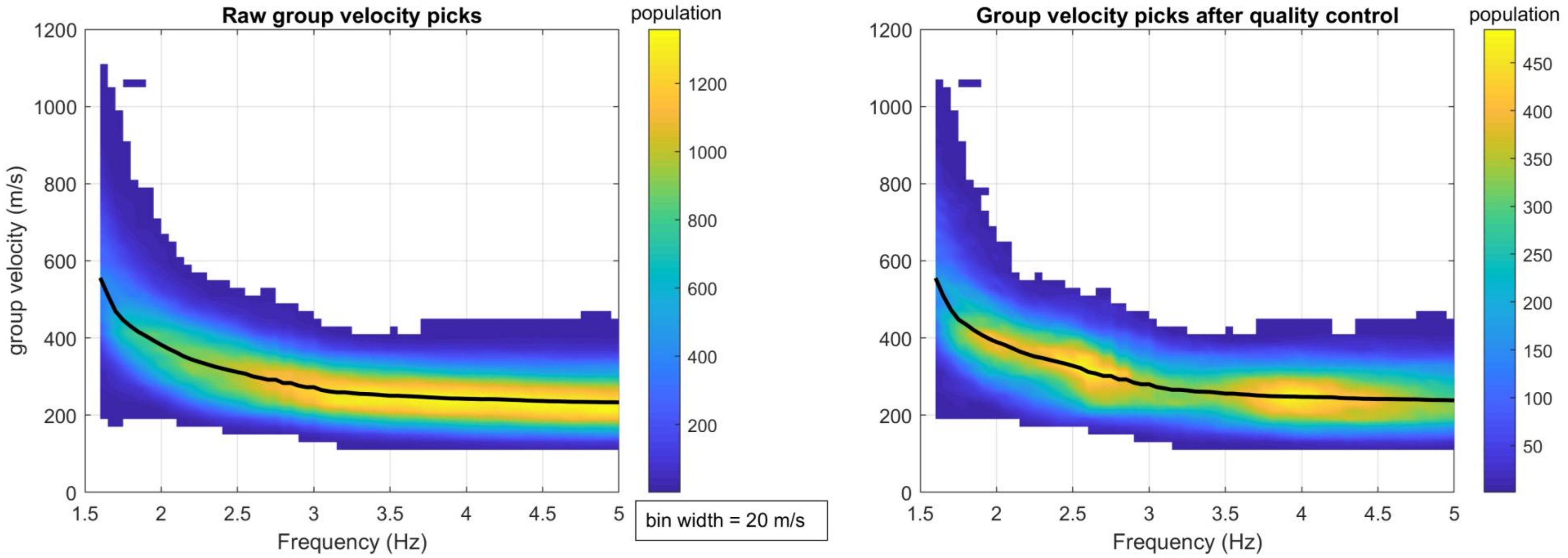

Fig16: (left) Histogram of group velocity picks in the frequency band 1.6 – 5.0 Hz. (right) same as left but after QC

Group velocity tomography performed with a grid size of 200 m

- This problem is reformulated as $\Delta t = G\Delta m$, where Δm is a perturbation in model around the mean slowness m_0
- $\Delta m = (\Delta t - Gm_0)^T C^{-1}(\Delta t - Gm_0) + m_0^T Q m_0$, where $Q = F^T F + H^T H$
- A detailed expansion of matrices F and H can be found in Barmin et al 2001
- We use smoothing parameters $\alpha = 4000, \beta = 300,$ and $\sigma = 200$ Goutorbe et al 2015

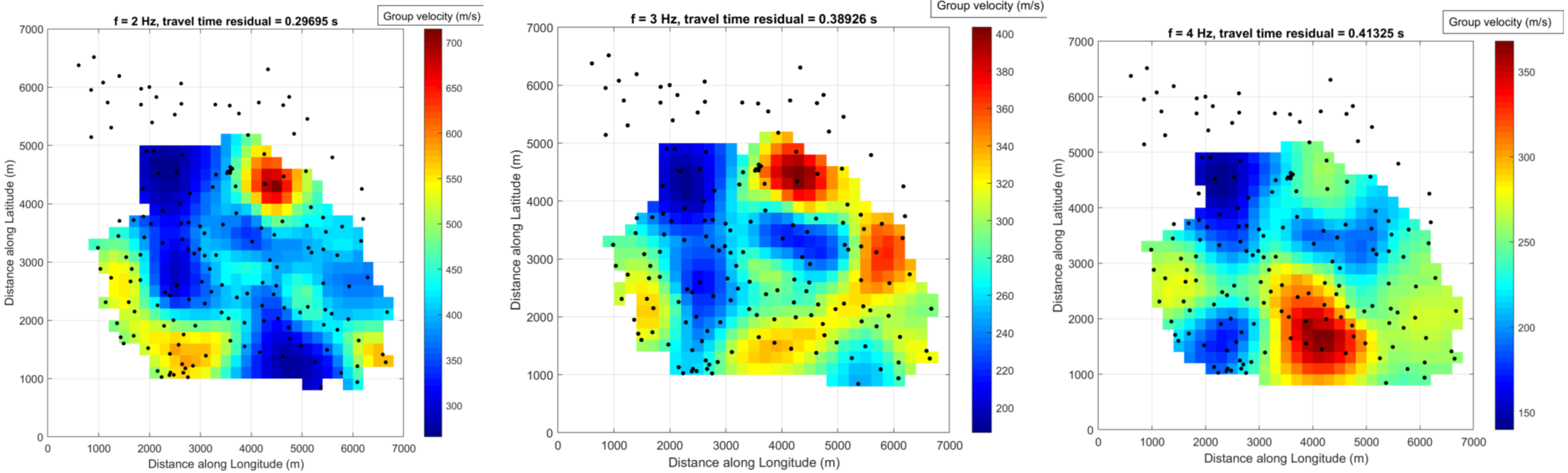

Fig17: Group velocity tomography results at frequencies 2 Hz, 3Hz, and 4 Hz

Tomography performance

- We evaluate the efficacy of the tomography in terms of
  - Variance reduction in travel-time $\approx 60 - 70\,\%$; a very good data set would give about 90% variance reduction
  - Spatial resolution $\approx 600m$

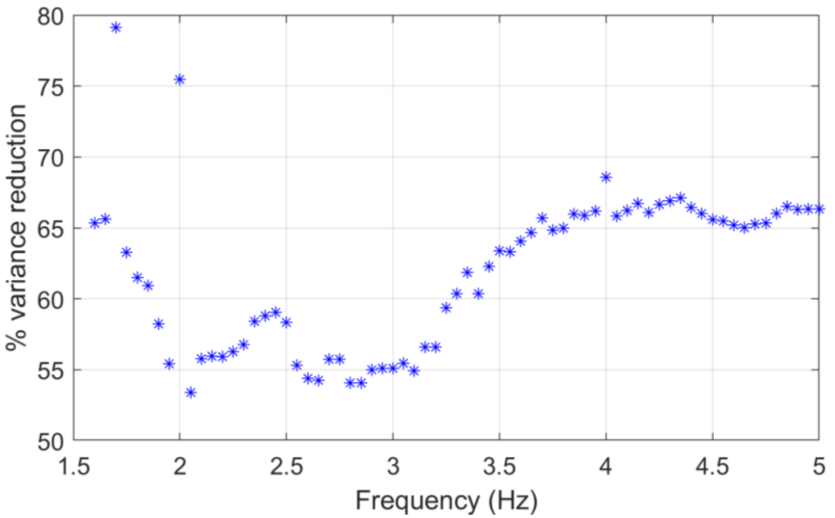

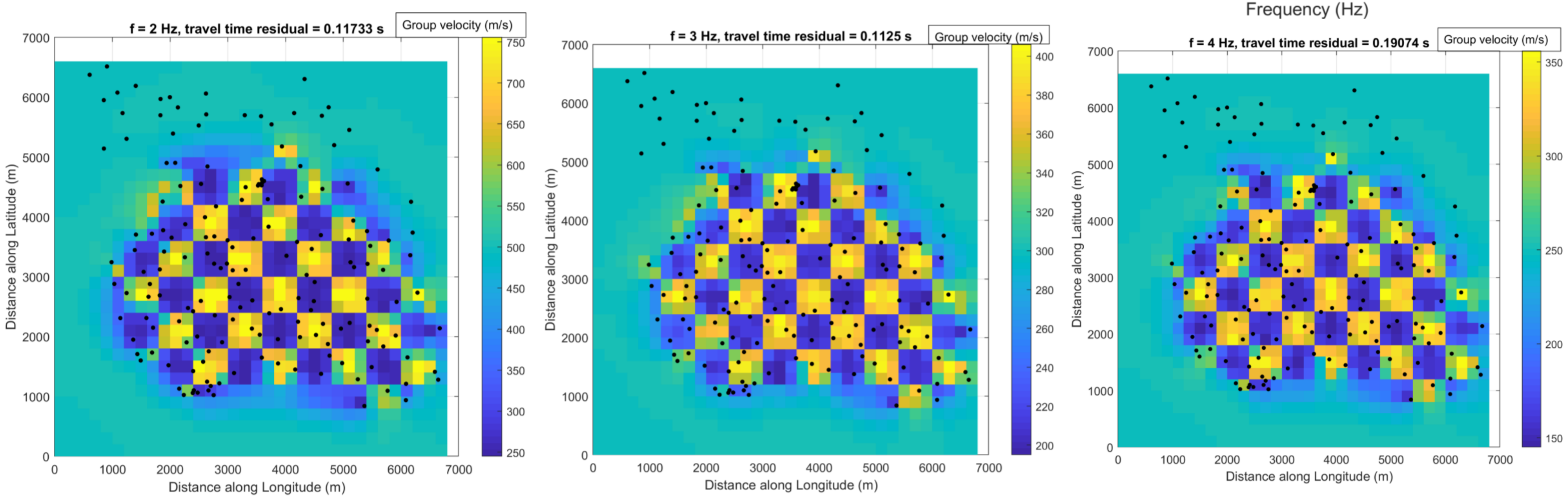

Fig18: Checkerboard test reveals a resolution of about 600 m; velocity variation were chosen based on tomography results of the field data

Depth inversion inputs and parameter space

- Inputs for the inversion of every grid points
  - Fundamental mode phase velocity1.6 -2.5 Hz - FK analysis – weights 0.5
  - First overtone phase velocity 1.4 – 2.0 Hz – FK analysis – weights 0.5
  - Group velocity fundamental mode – from tomography – weights 1.0
- Parameter space based on stratigraphy at site

Depth range (m)	P-wave velocity(m/s)	S-wave velocity (m/s)	Density (kg/m^3)	Poisson's ratio
0 – 50	500 - 1500	200 - 500	1200 - 1800	0.2 – 0.5
50 - 150	1000 - 5000	400 - 2000	1600 - 2000	0.2 – 0.4
100 - 300	1000 - 5000	500 - 2500	2000 - 2700	0.2 – 0.4
300 - 800	1000 - 5000	1000 - 3000	2000 - 2700	0.2 – 0.4
halfspace	3000 - 6000	3500 (fixed)	2000 - 2700	0.2 – 0.4

Table 1: Search range for the parameters Vp, Vs, density, Poisson's ratio and depth for the dispersion inversion

Depth inversion results

- Inversion results show a good correlation with topography
  - Clear indication of more soft-soil beneath the elevated regions in area of study
  - At depths of 300 m a velocity intrusion is observed beneath the elevated topography
  - Overall, in the valleys, changes to higher S-wave velocities between 50 -60 m
  - Beneath the hills, this occurs between 150 – 200 m

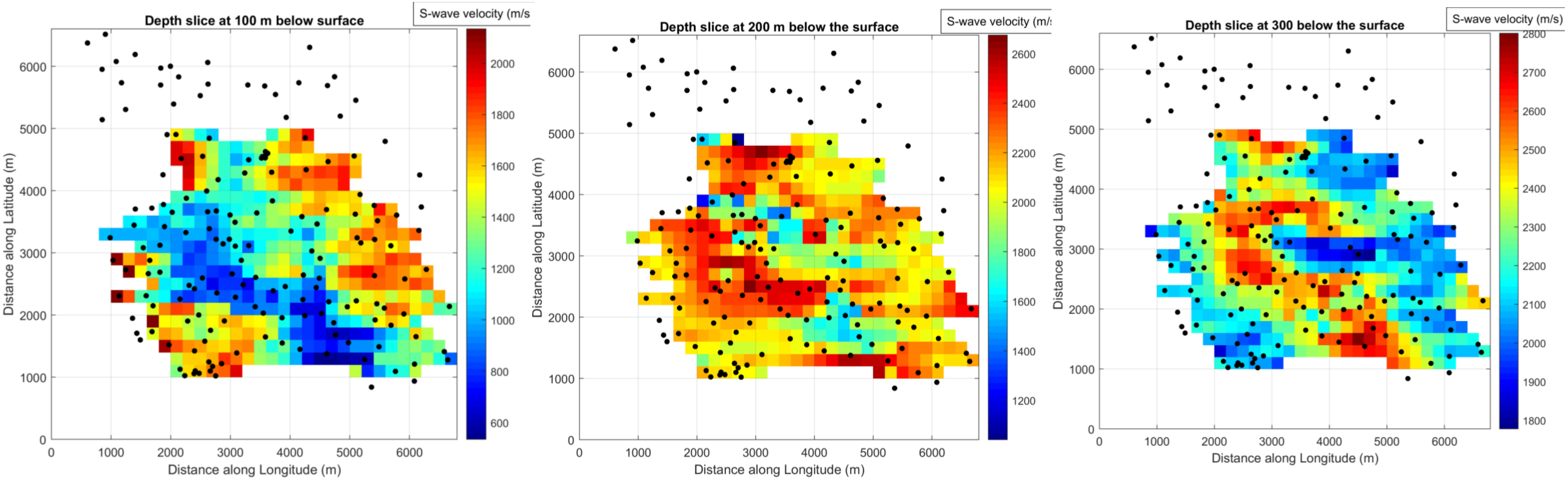

Figure 19: Depth slices of the distribution of S-wave velocities for depths of 100 m, 200 m, and 300 m from the local surface elevation

Depth inversion results – vertical velocity slices

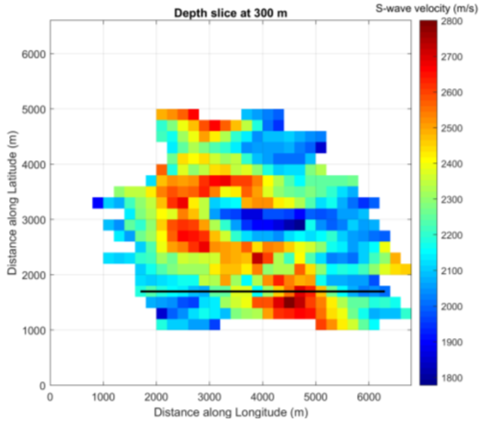

- Inversion results show a good correlation with topography
  - Overall, in the valleys, changes to higher S-wave velocities between 50 -60 m
  - Beneath the hills, this occurs between 150 – 200 m

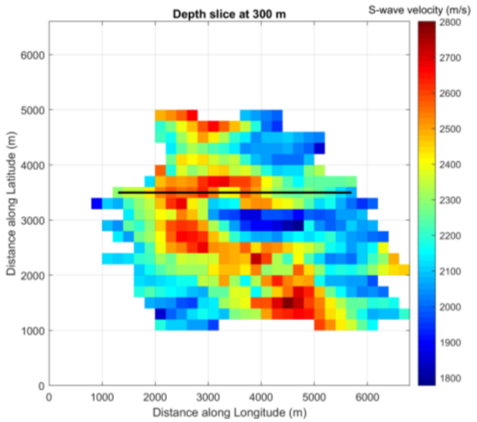

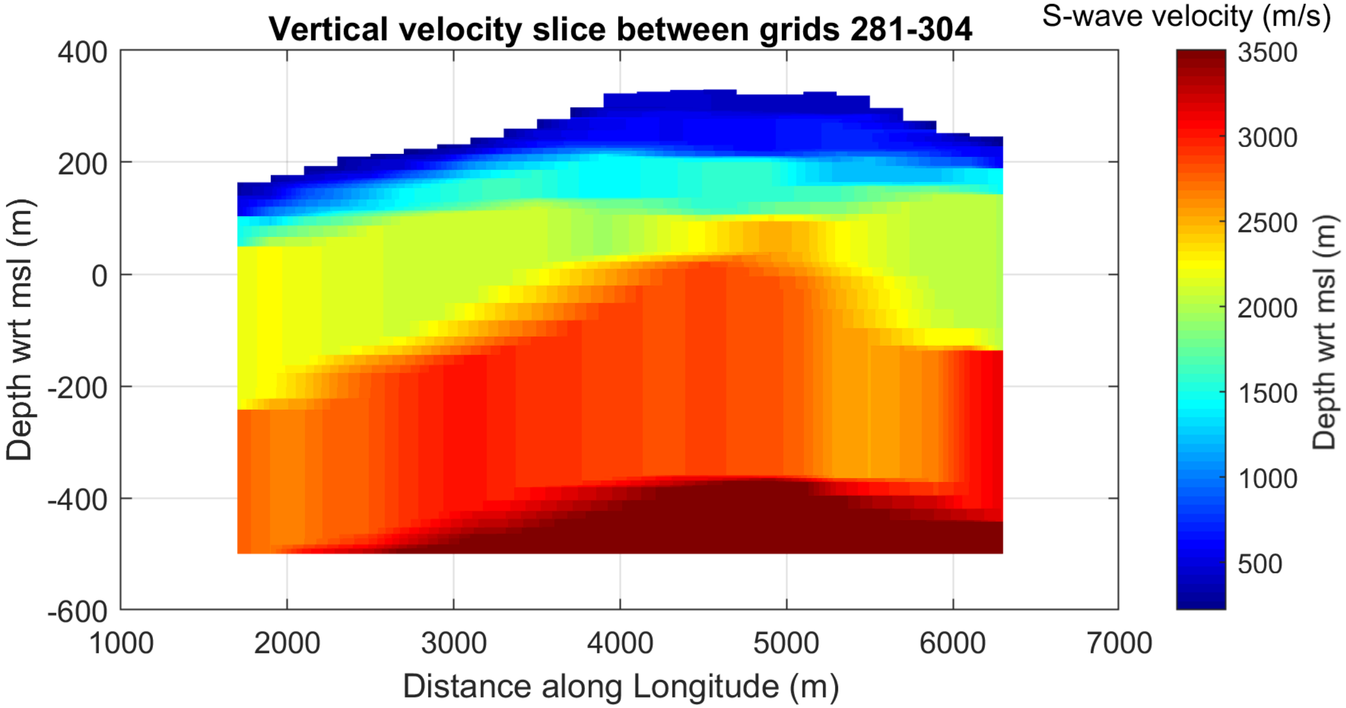

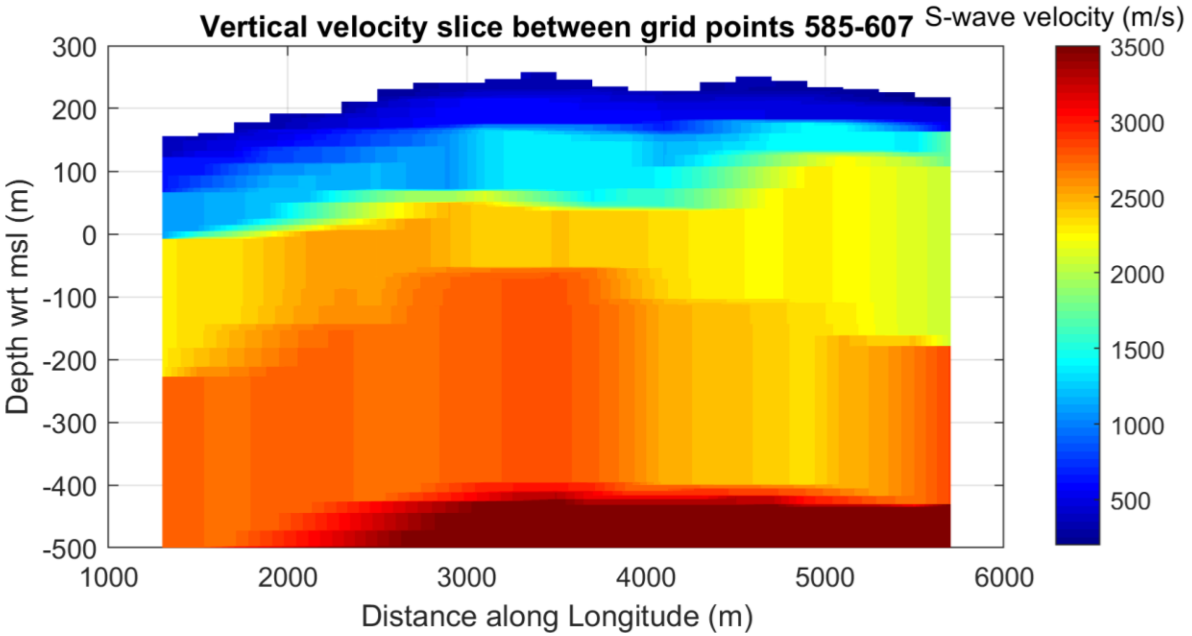

Figure 20: Vertical slices of the estimated S-wave velocities along grid 281-304, and 585-607

LIÈGE université

Conclusions

- Distribution of ambient surface seismic noise shows a reasonable correlation with surface topography
  - Valleys where hard rock is close to the surface show less surface seismic noise amplitudes due to lack of a reverberating medium
  - Regions with elevated topography show relatively stronger seismic noise but also shows correlation with distance from anthropogenic sources
- Rayleigh group and phase velocities show strong lateral variation, with much higher velocities observed in the valleys, and North of the array where different geological units are expected
- Regions with lower phase velocities shows a higher mode visible between 1.4 – 2.0 Hz
- Conversion of group velocity maps and regional phase velocity model show a good correlation with topography
  - Valleys are expected to have hard rock close to the surface
- Two major discontinuities are identified with depths dependent on the local surface elevation
  - Vaals (clay and sand) to Upper Cretaceous formation composed of soft limestones and sandstones
  - Namurian formation where S-wave velocities change from 1500 m/s to 2500 m/s
- Beyond 300 m, Dinantian/Fammenian formation composed of hard carstified limestones/hard micaceous limestone is expected with S-wave velocities increasing further to 3500 m/s